Generation of $\boldsymbol{E} \times \boldsymbol{B}$ flow shear by finite orbit width effects from heat sources in tokamaks

S. S. Kim[1]†, S. Ku[2], Hogun Jhang[1]

[1]Korea Institute of Fusion Energy, Daejeon 34133, Republic of Korea

[2]Princeton Plasma Physics Laboratory, Princeton University, Princeton, New Jersey 08543, USA

Abstract. We present a possible mechanism for the generation of strong $\boldsymbol{E} \times \boldsymbol{B}$ flow shear relevant to internal transport barrier formation in tokamak plasmas. From gyrokinetic calculations, we show that strong $\boldsymbol{E} \times \boldsymbol{B}$ flow shear can be generated by finite orbit width (FOW) effects associated with a non-uniform heat source and is sufficient to lead to transport barrier formation in the core region with a moderate power level. Two FOW effects inducing neoclassical polarization are shown to be responsible for this: 1) the radial drift of particle orbit center due to the variation of the heat source within orbit width and 2) the non-uniformly evolved orbit width by the non-uniform heating.

Keywords: $\boldsymbol{E} \times \boldsymbol{B}$ flow shear, internal transport barrier, heat source, finite orbit width effects

† sskim@kfe.re.kr

1. Introduction

Transport barrier formation is an important subject in magnetic fusion research [1, 2]. Since this phenomenon leads to a global confinement improvement, it has been an intense research field in magnetically confined plasmas. Experiments indicate that it is relevant to strong radial electric field ($\mathbf{E}_r$) generation [3]. The contemporary paradigm of transport barrier formation is based on turbulence decorrelation and stabilization by the subsequent strong $\boldsymbol{E}\times\boldsymbol{B}$ flow shear [3, 4].

To understand the physics of transport barrier formation, gyrokinetic (GK) approach has been used [5, 6]. The GK formulation [7, 8] has been a mature theoretical framework which can describe nonlinear dynamics of magnetized plasmas in the presence of self-consistent micro-scale electromagnetic fluctuations. The full-f GK simulation codes [9, 10, 11, 12, 13] with heat sources/sinks and self-consistently evolving plasma kinetic profiles have been developed intensively. However, in spite of the remarkable advancement in the GK simulations over the past decades, the unequivocal demonstration of the transport barrier formation with the generation of strong $\boldsymbol{E}\times\boldsymbol{B}$ flow shear is yet to be achieved.

The formation of an internal transport barrier (ITB) which refers to an improved confinement regime in the core region was initially associated with the formation of a reversed safety factor (q) profile [14, 15, 16]. However, there have been ample experimental observations that ITBs can form in the weak or positive q-profile shear when sufficiently strong power is applied to the plasma [17, 18]. This fact suggests that the q-profile shape might not be a sufficient condition for the ITB formation, requiring a physical origin likely related to the applied power itself. There has been no reliable physical explanation on this phenomenon, and it remains as one of long-standing problems in magnetic fusion research.

Reference [19] has shown that an additional vorticity source can be generated from a heat source through the finite Larmor radius (FLR) effects. Parra and Barnes [20] have provided a physical picture showing how finite orbit width affects radial electric field formation. A qualitative study in Ref. [20] has shown that a charge imbalance can be induced by the change of orbit widths due to energy injection, leading to a subsequent generation of a radial electric field. In this work, we study the finite orbit width (FOW) effect coupled with a heat source by analytically solving GK equation. From GK calculations, we show that a non-uniform heat source in tokamaks can induce substantial neoclassical polarization via the FOW effects. This, in turn, significantly enhances the undamped $\mathbf{E}_r$ [21] and its shear. The estimated value of the $\mathbf{E}_r$ shear due to a heat source with a moderate power level is shown to be significant enough to initiate an ITB formation. To support this finding, we present physics pictures which elucidate the origin of the $\boldsymbol{E}\times\boldsymbol{B}$ flow shear generation by the heat source. A rigorous calculation and the physics picture indicate that the $\mathbf{E}_r$ generation in Ref. [20] due to the change of orbit widths accounts only half of the total field by a heat source. The other half is shown to come from particle drifts caused by the variation of the heat source within

orbit width.

The remainder of this paper is organized as follows. In Sec. 2, we obtain the analytic solution of GK equation and calculate the electrostatic potential generated by the kinetic effect from a heat source. In Sec. 3, we investigate the FOW effect as the main physical origin of the potential or $\boldsymbol{E}\times\boldsymbol{B}$ flow shear generation and provide physics pictures elucidating the mechanisms of the FOW effect. The $\boldsymbol{E}\times\boldsymbol{B}$ flow shear predicted from the result in Sec. 2 is proportional to the applied heating power. Section 4 is devoted to the validation of the result in Sec. 2 and discussions on why the core confinement improvement does not gradually occur with increasing power but shows a threshold behavior. In Sec. 4.1, we present a simulation result using the XGC1 code [22] and compare it with the analytic result. In Sec. 4.2, we deal with the existence of threshold power for the ITB formation based on a heuristic model and estimate it in a typical L-mode condition. We conclude the paper in Sec. 5 with a brief summary of the main results and discussions on several future works.

2. Analytic calculation

In order to analytically show that an external heat source can generate $\boldsymbol{E}\times\boldsymbol{B}$ flow shear by FOW effects, we consider the following collisionless GK equation:

$$\left(\frac{\partial}{\partial t}+\mathcal{L}\right)f_1=-\frac{ef_0}{T_{i0}}\mathcal{L}\left(J_0\phi\right)+Q_E+Q_{ext}, \tag{1}$$

where $f_1=f_1(\mathbf{R}_g,w,\mu,t)$ is the perturbed part of the ion gyrocenter distribution $f=f_0+f_1$, $\mathcal{L}=\mathcal{L}_\parallel+\mathbf{v}_D\cdot\nabla$ with $\mathcal{L}_\parallel=v_\parallel\mathbf{b}\cdot\nabla$ and $\mathbf{v}_D=\dfrac{v_\parallel^2}{\Omega}\mathbf{b}\times(\mathbf{b}\cdot\nabla\mathbf{b})+\dfrac{\mu B}{m\Omega}\mathbf{b}\times\nabla\ln B$, J_0 is the gyroaveraging operator, ϕ is potential, $Q_E=-\mathbf{v}_E\cdot\nabla f_1$ with $\mathbf{v}_E=\dfrac{c}{B}\mathbf{b}\times\nabla\left(J_0\phi\right)$, and Q_{ext} represents an external heat source. Here, $\mathbf{R}_g$ is the gyrocenter position vector, $w=mv^2/2$, $\mu=mv_\perp^2/2B$, $|v_\parallel|=\sqrt{2(w-\mu B)/m}$, $\mathbf{b}=\mathbf{B}/B$, $\Omega=eB/mc$, and f_0 is Maxwellian with density n_0 and ion temperature T_{i0}. Taking the axisymmetric part of Eq. (1) and using $\mathbf{v}_D\cdot\nabla\hat{F}=i\mathbf{v}_\parallel\cdot\nabla\Theta\hat{F}$, we have

$$\left(\frac{\partial}{\partial t}+\mathcal{L}_\parallel\right)\left(e^{i\Theta}\hat{f}_1\right)=-\mathcal{L}_\parallel\left(\frac{ef_0}{T_{i0}}e^{i\Theta}J_0\langle\phi\rangle\right)+e^{i\Theta}\hat{Q}, \tag{2}$$

where $\hat{F}$ denotes the axisymmetric part of a physical quantity F, $\hat{\phi}=\langle\phi\rangle$ is assumed with $\langle F\rangle$ a flux-surface average of F, $\hat{Q}=\hat{Q}_E+\hat{Q}_{ext}$, and

$$\Theta=k_r\Lambda\ \text{ with }\ \Lambda=\frac{Iv_\parallel}{\psi'\Omega} \tag{3}$$

measures the radial orbit width normalized by the radial wavelength [23]. In Eq. (3), k_r is the radial wavenumber, $I=RB_T$ with R the major radius and B_T the toroidal magnetic field, and $\psi'=\partial\psi/\partial r$ with ψ the poloidal flux function. One can solve Eq. (2) perturbatively considering only slowly varying long-time evolution so that $\mathcal{L}_\parallel$ is a leading order operator [21, 23]. The result is given by

$$\hat{f}_1=\frac{ef_0}{T_{i0}}\left(e^{-i\Theta}\overline{e^{i\Theta}J_0\left\langle\phi\right\rangle}-J_0\left\langle\phi\right\rangle\right)+e^{-i\Theta}\overline{e^{i\Theta}\hat{W}}, \tag{4}$$

where $\overline{F} = \oint F v_\parallel^{-1} dl / \oint v_\parallel^{-1} dl$ with dl the line element along the field line. In Eq. (4), $\hat{W} = \hat{f}_1(t=0) + \int_0^t (\hat{Q}_E + \hat{Q}_{ext}) dt'$, and the term $\hat{f}_1(t=0)$ representing an initial condition and the nonlinear term involving $\hat{Q}_E$ play a role of the source in the generation of residual flows which are undamped by linear collisionless processes [21, 23]. In this study, we show that the external heating can provide another source for the residual flow. An advantage of this source is that it is controllable in experiments with heating conditions such as heating profile and power, in contrast to other sources.

For simplicity, we consider only the heat source contribution to $\hat{W}$ in calculating the potential $\langle\phi\rangle$ from Eq. (4). The effect of nonlinear convection will be discussed in Sec. 4.2. We use $Q_{ext} = J_0 \vartheta_{ext}$ with ϑ_{ext} an external source representing creation and annihilation of particles in particle phase space by heating [19]. As a model for ϑ_{ext}, we use the following form [10],

$$\vartheta_{ext} = \frac{G_{src}(r)}{\tau_{src}} (f_{M2} - f_{M1}), \tag{5}$$

where f_{Mj} is Maxwellian with density n_c and temperature T_{cj} ($j = 1$ or 2). Here, τ_{src}, n_c, and T_{cj} are some constants. The input heating power is given by $P_{in} = \int \frac{3}{2} S_H d\mathbf{r}$, where $S_H(r) = \frac{G_{src}}{\tau_{src}} n_c (T_{c2} - T_{c1})$ denotes a heat source profile. Then, from Eqs. (4) and (5), the flux-surface average of the perturbed gyrocenter density is given by

$$\langle n_1 \rangle = -\frac{e n_0 \xi_{neo}}{T_{i0}} \langle\phi\rangle - \frac{\left(\xi_{neo} + \frac{1}{2}\xi_{cl}\right)}{T_{i0}} \int_0^t S_H dt', \tag{6}$$

where $\xi_{neo} = n_0^{-1} \left\langle \int d^3v f_0 \left(\overline{\Theta^2} - \overline{\Theta}^2 \right) \right\rangle$, $\xi_{cl} = \langle k_r^2 \rho_i^2 \rangle$ with $\rho_i = \Omega^{-1}\sqrt{T_{i0}/m}$, and we have assumed $\left(\Theta - \overline{\Theta}\right)^2 \ll 1$. Using the quasi-neutrality [8], $\langle n_1 \rangle + \left\langle n_{pol}^{cl} \right\rangle = 0$ with $\left\langle n_{pol}^{cl} \right\rangle = -(\xi_{cl}/T_{i0}) (e n_0 \langle\phi\rangle + \Delta p_i/2)$, and Eq. (6), we obtain

$$\frac{e n_0 \mathcal{D}}{T_{i0}} \langle\phi\rangle = -\frac{\mathcal{D}}{T_{i0}} \int_0^t S_H dt', \tag{7}$$

where $\mathcal{D} = \xi_{cl} + \xi_{neo}$, $p_{i0} = n_0 T_{i0}$, and $\Delta p_i = \int_0^t S_H dt'$.

Equation (7) is the main result of this work. It implies that a heat source can be a strong driver of the residual flow. For large aspect ratio circular geometry, the expression for $\mathcal{D}$ is well-known as $\mathcal{D} = \langle k_\perp^2 \rho_i^2 \rangle \left(1 + 1.6 q^2 \epsilon^{-1/2}\right)$ [21], where $q = \epsilon B/B_P$ with B_P the poloidal field and $\epsilon = r/R_0$ with R_0 the major radius on the magnetic axis. When we include the initial term, its contribution to the right hand side of Eq. (7) is given by $(e n_0 \xi_{cl}/T_{i0}) \langle\phi(t=0)\rangle$. The electrostatic potential by the initial term and the heat source is then given by $\langle\phi\rangle = (\xi_{cl}/\mathcal{D}) \langle\phi(t=0)\rangle$ and $\langle\phi\rangle = -(1/e n_0) \int_0^t S_H dt'$, respectively. Considering $\xi_{cl}/\mathcal{D} = \left(1 + 1.6 q^2 \epsilon^{-1/2}\right)^{-1} \sim 0.1$ for typical tokamak parameters and assuming $(1/e n_0) \int_0^t S_H dt' \sim |\langle\phi(t=0)\rangle|$, the undamped residual flow can be significantly enhanced by an external heat source compared to the case only with the initial term.

3. Physical origin of $\boldsymbol{E}\times\boldsymbol{B}$ flow shear generation

In Eqs. (6) and (7), terms with ξ_{cl} and ξ_{neo} represent classical and neoclassical contributions, respectively. The classical term associated with the heat source results from the FLR effects [19]. The neoclassical term, which is the main focus in this paper, is attributed to the FOW effects in toroidal geometry. To elucidate its physical origin, we consider a trapped or passing particle moving along a bounce- or transit- orbit with $r = r_c + \delta r$ as shown in Fig. 1(a) or (b), where r_c and δr represent orbit center and width, respectively. We define r_c by $\psi(r_c, t) = \{\psi\}$ and δr is approximately given by

$$\delta r = \Lambda - \overline{\Lambda} \tag{8}$$

from $\psi'\delta r \simeq \psi - \{\psi\} = Iv_\parallel/\Omega - I\overline{v_\parallel/\Omega}$ when $dp_\zeta/dt = 0$, where $p_\zeta = mIv_\parallel/B - e\psi/c$ is the canonical angular momentum, $\{\cdot\}$ denotes orbit-average along the particle trajectory, and we have used $\{Iv_\parallel/\Omega\} = I\overline{v_\parallel/\Omega}$. We note that $\{F\} = \overline{e^{ik_r\delta r}F}$ with $\overline{(\cdot)}$ performed on $r = r_c$ flux surface and $k_r = 0$ except for $F = \langle\phi\rangle$ or S_H. Using Eq. (8), we have $\Theta - \overline{\Theta} = k_r\delta r$ and $\xi_{neo} = n_0^{-1}\left\langle \int d^3v f_0 k_r^2 \overline{\delta r^2}\right\rangle$, which contain the FOW effects. Now, we assume that an external force $\mathbf{F}_{ext}$ provides energy input s_h to the particle with a radially decreasing profile nearby $r = r_c$. From $s_h = \mathbf{v}\cdot\mathbf{F}_{ext}$, one may represent it as

$$\mathbf{F}_{ext} = \frac{\mathbf{v}}{v^2}s_h(r). \tag{9}$$

The model force in Eq. (9) is isotropic and the net force exerted on a fluid element by it is zero when the given distribution is isotropic. Even in this case, however, particle flow can arise by kinetic effects if s_h is radially non-uniform. The gyroaverage of the perpendicular component of $\mathbf{F}_{ext}$ affecting particle gyromotion leaves a net force in poloidal direction giving rise to a drift when $\partial s_h/\partial r \neq 0$ [19]. In this work, we consider the parallel component of $\mathbf{F}_{ext}$ affecting the particle guiding-center motion. One can expand it near $r = r_c$ as $F_{ext\parallel} \simeq F_{ext\parallel,c} + \delta F_{ext\parallel}$, where

$$F_{ext\parallel,c} = \frac{v_\parallel}{v^2}s_h(r_c) \text{ and } \delta F_{ext\parallel} = \frac{v_\parallel}{v^2}\delta r\left.\frac{\partial s_h}{\partial r}\right|_{r=r_c}. \tag{10}$$

First, we evaluate the change in δr by $F_{ext\parallel}$. We assume that $F_{ext\parallel}$ is much weaker than the mirror force $F_m = -\mu\mathbf{b}\cdot\nabla B$ and the deformation of an orbit by $F_{ext\parallel}$ during δt is small, where δt is the bounce- or transit-time when $F_{ext\parallel} = 0$. Consider a particle starting from outer midplane at time $t_0 = 0$. It passes through there at successive times $t = t_1,\ t_2,\ \cdots$ and so on. We define the jth orbit as a particle trajectory for $t_j \le t \le t_{j+1}$ and the orbit-average for it as $\{F\}_j = \delta t_j^{-1}\int_{t_j}^{t_{j+1}} F dt$ with $\delta t_j = t_{j+1} - t_j \simeq \delta t$, where the integral is performed along the particle trajectory. We also define a slowly varying smooth function $\{F\}(t)$ as one satisfying $\{F\}(t_j + \delta t_j/2) = \{F\}_j$ for all j and use it as an orbit-average of F. Now, $F_{ext\parallel}$ provides an effective torque $\mathcal{T}_{eff} = IF_{ext\parallel}/B$. Then, from $dp_\zeta/dt = \mathcal{T}_{eff}$, δr has an additional term, $-(c/e\psi')A(t)$, where $A(t) = \int_0^t \mathcal{T}_{eff}dt' - \{\int_0^t \mathcal{T}_{eff}dt'\}$. Note that $A(t)$ is zero at $t = t_1,\ t_2,\ \cdots$ from $\int_0^{t_j} F dt' = \{\int_0^{t_j} F dt'\}$ and does not retain the effect of $F_{ext\parallel}$ during particle excursions in the previous orbits. When $F_{ext\parallel}$ is much weaker than F_m, one can neglect this extra

term and use δr in Eq. (8). To evaluate the long-time evolution of δr, we assume that the increment of δr for $t = \Delta t \gg \delta t$ is still small and $\Delta(\delta r)/\delta r \simeq \Delta w_\parallel / 2\overline{w_\parallel} \ll 1$, where Δ represents the increment after the external source is applied and $w_\parallel = m v_\parallel^2/2$. Under this assumption, $\Delta(\delta r)$ can be estimated as

$$\Delta(\delta r) = \frac{\delta r}{m v^2} \int_0^t s_{h,c} dt', \tag{11}$$

where $s_{h,c} = s_h(r_c)$ and we have used

$$\Delta w_\parallel \simeq \int_0^t \frac{v_\parallel^2}{v^2} s_{h,c} dt' \simeq \frac{\overline{w_\parallel}}{w} \int_0^t s_{h,c} dt'. \tag{12}$$

Equation (11) describes the increase of orbit width or shift for a trapped or a passing particle by $F_{ext\parallel,c}$. On the other hand, $\delta F_{ext\parallel}$ induces a change in r_c and therefore particle drift. To show this, we first consider a trapped particle. In this case, $\delta F_{ext\parallel}$ in Eq. (10) acts on the particle in the opposite (same) direction to the bounce motion when $r > r_c$ ($r < r_c$) as shown in Fig. 1(a). When the particle moves toward upper (lower) point in $r > r_c$ ($r < r_c$) region, it bounces earlier (later) at radially outer position due to the decelerating (accelerating) parallel force compared to the case of $\delta F_{ext\parallel} = 0$ (i.e., uniform s_h). As a result, both upper and lower bounce points move outward in radial direction, giving rise to outward polarization. We calculate the drift velocity of bounce center by using a bounce orbit-average of $\mathcal{T}_{eff}$,

$$\{\mathcal{T}_{eff}\} = \frac{I}{v^2} \frac{\overline{v_\parallel \delta r}}{B} \frac{\partial s_h}{\partial r}, \tag{13}$$

where we have used $\overline{v_\parallel/B} = 0$ for the trapped particle. Then, we have

$$\frac{d\{\psi\}}{dt} = \frac{\partial \psi}{\partial r_c}\frac{dr_c}{dt} + \frac{\partial \psi}{\partial t} = -\frac{c}{e}\{\mathcal{T}_{eff}\}, \tag{14}$$

where we have used $d\{p_\zeta\}/dt \simeq \{dp_\zeta/dt\} = \{\mathcal{T}_{eff}\}$ and $\{\psi\} = \psi(r_c, t)$ with $r_c = r_c(t)$ denoting the moving bounce center. From Eqs. (13) and (14), we obtain

$$\frac{dr_c}{dt} = u_d + u_s \quad \text{with} \quad u_d = -\frac{\overline{\delta r^2}}{m v^2}\frac{\partial s_h}{\partial r}, \tag{15}$$

where u_d is the bounce center drift velocity driven by the FOW effect from an external heat source and $u_s = -(1/\psi')\partial\psi(r_c,t)/\partial t = -(c/\psi')\overline{RE_T}$ represents the Ware pinch [24] with E_T the toroidal electric field.

Similarly, one can calculate the outward drift velocity of a passing particle due to $\delta F_{ext\parallel}$ as shown in Fig. 1(b). The transit orbit-average of $\mathcal{T}_{eff}$ gives

$$\frac{d}{dt}\left(mI\frac{\overline{v_\parallel}}{B} - \frac{e}{c}\{\psi\}\right) = \frac{I}{v^2}\frac{\overline{v_\parallel}}{B} s_{h,c} + \frac{I}{v^2}\frac{\overline{v_\parallel \delta r}}{B}\frac{\partial s_h}{\partial r}. \tag{16}$$

Since $\delta F_{ext\parallel} (\propto \delta r)$ oscillates during a particle circulation, $\Delta w_\parallel$ by it is negligible. Using $\Delta(mI\overline{v_\parallel/B}) \simeq (\Delta w_\parallel/2\overline{w_\parallel}) mI\overline{v_\parallel/B}$, the net change in toroidal angular momentum by $\delta F_{ext\parallel}$ during Δt is also negligible. Then, the toroidal angular momentum of passing particle changes mainly by $F_{ext\parallel,c}$ and E_T, i.e., $\frac{d}{dt}\left(mI\frac{\overline{v_\parallel}}{B}\right) \simeq \frac{I}{v^2}\frac{\overline{v_\parallel}}{B} s_{h,c} + e\overline{RE_T}$.

Employing this approximation and Eq. (16), the radial drift velocity of the passing particle is given by u_d in Eq. (15).

The time evolution of gyrocenter density increment induced by this drift is given by

$$\frac{\partial\langle\Delta n\rangle}{\partial t} = -\langle\nabla\cdot\boldsymbol{\Gamma}_d\rangle = -\frac{\xi_{neo}}{2T_{i0}}S_H, \tag{17}$$

where $\boldsymbol{\Gamma}_d = \int d^3v f_0 u_d\hat{\mathbf{r}}$ and we have used $s_h = (3/2n_0)S_H$ and $\left\langle \int d^3v f_0 k_r^2\overline{\delta r^2}/mv^2\right\rangle = \xi_{neo}n_0/3T_{i0}$. Equation (17) implies that the drifts of trapped and passing particles induced by $\delta F_{ext\|}$ are responsible for the half of the neoclassical polarization induced by a heat source in Eq. (6) or (7).

To find the origin of the remaining half in Eq. (7), we consider ions moving nearby a reference position $r = r_p$ as shown in Fig. 2, which determine the ion density at $r = r_p$. Polarization can be induced if δr of the ions changes non-uniformly. As S_H changes from uniform to non-uniform one with $\partial S_H/\partial r < 0$ near $r = r_p$, the orbit width (shift) of the trapped (passing) particles coming from $r < r_p$ or $r > r_p$ region increases or decreases, leading to the net outward shift of ions from $r = r_p$. The polarization at $r = r_p$ by the change in δr, $\Delta(\delta r)$, can be estimated as

$$\Delta\mathbf{P} = e\int d^3v f_0\Delta(\delta r)\hat{\mathbf{r}}. \tag{18}$$

Substituting Eq. (11) into (18) and using $s_h(r_c) \simeq (3/2n_0)\left[S_H(r_p) - \delta r\left(\partial S_H/\partial r\right)\right]$, we obtain the time evolution of $\langle\Delta n\rangle$ by the change in δr as

$$\frac{\partial\langle\Delta n\rangle}{\partial t} = -\frac{1}{e}\left\langle\nabla\cdot\frac{\partial\Delta\mathbf{P}}{\partial t}\right\rangle = -\frac{\xi_{neo}}{2T_{i0}}S_H. \tag{19}$$

Therefore, we identify that the other half of the neoclassical contribution from a heat source in Eq. (7) comes from the polarization by the non-uniformly evolved δr.

4. Simulation result and discussions

4.1. Comparison between simulation and analytic results

From Eq. (7), the increment in radial electric field by the non-uniform heat source is given by

$$\Delta E_r^H = \frac{1}{en_0}\int_0^t\frac{\partial S_H}{\partial r}dt' \tag{20}$$

in the collisionless case. The subsequent $\boldsymbol{E}\times\boldsymbol{B}$ shearing rate, $\omega_E^H = \left|(c/B_0)\partial\Delta E_r^H/\partial r\right|$, is then proportional to the heating power per particle in the heated region and the profile curvature of heat source. To validate the result in Eq. (20), we perform a GK simulation using the XGC1 code [22] without turbulence and collisions. It is carried out for $\Delta t = 0.49$ ms in a circular geometry with minor radius $a = 0.6$ m, $R_0 = 1.7$ m, and $B_0 = 1.9$ T. The heat source has a Gaussian-like profile peaked at $r = 0.55a$. We use $P_{in} = 6.9$ MW and monotonic profiles for n_0 and T_{i0} with $n_0 = 3.9\times10^{19}\mathrm{m}^{-3}$ and

$T_{i0} = 885$ eV at $r = 0.5a$. Figure 3 shows the simulation (blue) and analytic (orange) results of the $\boldsymbol{E} \times \boldsymbol{B}$ shearing rate ω_E^H. In the simulation, since we use 4 stacked trapezoids to meet the radial heating profile requirement of XGC1, sudden changes of derivative of S_H exist and give rise to the wiggles of ω_E^H in Fig. 3. In the analytic calculation, we employ a more smooth profile fitted with a Gaussian from S_H of the simulation. Considering the difference in S_H between the two calculations, the overall trend of the simulation result shows good agreement with the analytic one.

4.2. Estimation of threshold power for ITB formation

Many tokamak experiments indicate that the threshold power exists for ITB formation [1, 25, 26, 27]. A notable feature here is that the input power per particle is an important parameter for the ITB formation [26], which is consistent with the result in Eq. (20). In Sec. 4.2, we make a heuristic analysis on the existence of power threshold to overcome the L-mode confinement scaling. In our analysis, the increase of power is always likely to entail the confinement improvement due to the generation of stronger ω_E^H. This looks to be contradictory to the L-mode scaling where core confinement degrades as heating power increases [28]. To resolve this issue, we first note that the actual S_H should be replaced with $S_H^{eff} = S_H - S_{turb}$, where S_{turb} represents a heat loss by turbulent convection. The point is that turbulence also increases as heating power does. We note that S_{turb} originates from the nonlinear $\boldsymbol{E} \times \boldsymbol{B}$ convection term Q_E in Eq. (1). To show the existence of power threshold, S_{turb} should be represented as a function of the heat source and the radial electric field involving nonlinear dynamics. In this work, we employ the transport model $S_{turb} = S_L/(1 + \omega_E^2/\gamma_{lin}^2)$ given by Hinton [29], where ω_E represents the net $\boldsymbol{E} \times \boldsymbol{B}$ shearing rate, γ_{lin} is the linear growth rate of an instability, and $S_L = -n_0\chi_L\nabla_\perp^2 T_i$ with χ_L the turbulent thermal diffusivity when $\omega_E = 0$. We consider a situation where the temperature gradient reaches the critical one giving rise to an instability with a low power at $t = 0$. We assume that $S_{turb} = S_H$ with $\omega_E = 0$ or $S_L = S_H$ at $t = 0$. Now we begin to increase the power in the L-mode condition. Under the assumption that S_L is proportional to the heating power, $S_L = S_H$ still holds. Using $S_{turb} = S_H/(1 + \omega_E^2/\gamma_{lin}^2)$, we develop a heuristic model for ω_E evolution.

When ion-ion collision is retained, one can set up an evolution equation for ω_E^H as $\partial\omega_E^H/\partial t = \alpha_H - (\omega_E^H - \omega_{E0})/\tau_c$ in the absence of turbulence, where α_H denotes a source for the $\boldsymbol{E}\times\boldsymbol{B}$ flow shear by the heat source effect, τ_c is an effective collision time, and ω_{E0} represents mean flow shearing rate [30]. From the time derivative of Eq. (20), the source α_H is given by $\alpha_H = (c/en_0B_0)\,|\partial^2 S_H/\partial r^2|$. In the presence of turbulence with $S_L = S_H$, the time evolution of ω_E can be described by $\partial\omega_E/\partial t = \alpha_H^{eff} - (\omega_E - \omega_{E0})/\tau_c + \Gamma_{NL}$ or

$$\frac{\partial\omega_E}{\partial t} = -\frac{\omega_E}{\tau_c\,(\omega_E^2 + \gamma_{lin}^2)}\left(\omega_E^2 - \omega_{Ec}^H\omega_E + \gamma_{lin}^2\right) + \frac{\omega_{E0}}{\tau_c} + \Gamma_{NL}, \tag{21}$$

where $\alpha_H^{eff} = (c/en_0B_0)\left|\partial^2 S_H^{eff}/\partial r^2\right|$ denotes effective α_H reduced by turbulent heat loss, Γ_{NL} represents a source by nonlinear interactions, and $\omega_{Ec}^H = \tau_c\alpha_H$ is the saturated value of ω_E^H when only collisions are retained. In Eq. (21), we have used

$S_H^{eff} = S_H - S_{turb} = S_H\left[1-(1+\omega_E^2/\gamma_{lin}^2)^{-1}\right]$ and $\alpha_H^{eff} \simeq \left[1-(1+\omega_E^2/\gamma_{lin}^2)^{-1}\right]\alpha_H$. For the sake of simplicity, we first neglect the last two terms of the right hand side in Eq. (21). In order to have non-zero ω_E at a steady state, $\omega_{Ec}^H \geq 2\gamma_{lin}$ should be met. This leads to $\omega_E \geq \gamma_{lin}$, which corresponds to the turbulence quenching condition [31, 32]. Figure 4 shows $y = (\tau_c/\gamma_{lin})\,\partial\omega_E/\partial t$ as a function of $x = \omega_E/\gamma_{lin}$ given from Eq. (21). In Fig. 4, the dashed line represents the case $\eta \equiv (\omega_{E0} + \tau_c\Gamma_{NL})/\gamma_{lin} = 0$ with $\omega_{Ec}^H = 2\gamma_{lin}$. The inclusion of finite ω_{E0} and Γ_{NL} can induce a bifurcation-like increase in ω_E satisfying the steady state condition $\partial\omega_E/\partial t = 0$ at $\omega_{Ec}^H \gtrsim 2\gamma_{lin}$. For example, the solid lines in Fig. 4 show the behavior of y as $z = \omega_{Ec}^H/\gamma_{lin}$ increases from 0 to 1.7 when $\eta = 0.18$. In this case, ω_E satisfying $y = 0$ remains a low level ($\omega_E/\gamma_{lin} \simeq 0.2 - 0.3$) until ω_{Ec}^H or the power reaches a threshold value ($\omega_{Ec}^H \simeq 1.65\gamma_{lin}$), then makes a transition to a high value ($\omega_E \simeq \gamma_{lin}$), exhibiting a feature of bifurcation.

As a next step, we estimate the necessary power for the ITB formation. Based on the heuristic model described by Eq. (21), the transition condition can be written as $\omega_{Ec}^H \geq c_T\gamma_{lin}$, where c_T is a constant $\left(\lesssim 2\right)$ depending on η. Since $\omega_{Ec}^H \propto \tau_c$, the effective collision time τ_c is an important parameter in determining the threshold power for the ITB transition. Using $\tau_c = 1.5\epsilon\tau_{ii}$ [33] with τ_{ii} the ion-ion collision time, we evaluate $\omega_{Ec}^H = \tau_c\alpha_H$ in the Cyclone case [34, 35]. For L-mode profiles, we use $n_0 = n_{0c}\exp\left[-\frac{\Delta_r}{L_n}\tanh\left(\frac{r-0.5a}{\Delta_r}\right)\right]$, $T_{i0} = T_{i0c}\exp\left[-\frac{\Delta_r}{L_{T_i}}\tanh\left(\frac{r-0.5a}{\Delta_r}\right)\right]$, and $q = 0.854 + 2.184(r/a)^2$ with $n_{0c} = 2\times10^{19}$ m^{-3}, $T_{0c} = 2$ keV, $\Delta_r/a = 0.3$, $R_0/L_n = 2.22$, $R_0/L_{T_i} = 6.92$, $a = 0.48$ m, $R_0 = 1.3$ m, and $B_0 = 1.9$ T as in Ref. [35]. These give $\rho_* = \rho_i/a = 0.007$, $\epsilon = 0.18$, $q = 1.4$, and $d(\ln T_{i0})/d(\ln n_0) = L_n/L_{T_i} = 3.1$ at $r = 0.5a$. Under the Cyclone base conditions, the orbit width of trapped particles and the effective collision time (τ_c) are given by $\delta r \sim q\epsilon^{-1/2}\rho_i = 0.023a$ and $\tau_c = 1.9$ ms at $r = 0.5a$, respectively. To examine the applicability of our model to actual experiments, we investigate the $\boldsymbol{E}\times\boldsymbol{B}$ flow shear generation by a model off-axis heat source with a Gaussian profile. Figure 5 shows n_0, T_{i0}, q, and S_H used in this exercise. In experiments, the monotonic increase of q may not be consistent with the off-axis heating. A quantitative calculation with compatible equilibrium profiles remains as a future work and we here give a rough estimation of the threshold power for the ITB formation. The model heat source in Fig. 5 is possibly to be implemented in actual experiments: e.g., one can find heating profiles with similar scale lengths for ITB discharges in JT-60U (see figure 25 in Ref. [27]). For a Gaussian heat source $S_H = S_0 e^{-(r-r_0)^2/2\sigma^2}$, ω_{Ec}^H has local maximum values at r_0 and $r_\pm = r_0 \pm \sqrt{3}\sigma$. In a reversed-$q$ case, r_+ is likely to be near q-minimum position. We take r_+ as an important location and estimate ω_{Ec}^H there. With $r_0 = 0.3a$ and $\sigma = 0.12a$, which has been used for S_H in Fig. 5, we have $\omega_{Ec}^H \geq 1.26\times10^5$ s^{-1} for $P_{in} \geq 4.7$ MW at $r = r_+$. In Fig. 5, ω_{Ec}^H for $P_{in} = 4.7$ MW is presented as a blue line. The linear growth rate for the Cyclone case is $\gamma_{lin} = 6.3\times10^4$ s^{-1} [35]. Then, from the transition condition, the heat source alone without regard to the q-profile can lead to the ITB formation near $r_+ \simeq 0.5a$ by inducing sufficient $\boldsymbol{E}\times\boldsymbol{B}$ flow shear with a moderate power level: in case of a heat source profile with a smaller

curvature such as central heating, a higher power is necessary for the ITB formation.

5. Concluding remarks

In summary, we have shown from a gyrokinetic calculation that the finite orbit width effects coupled with a radially non-uniform heat source can induce significant $\boldsymbol{E}\times\boldsymbol{B}$ flow shear. Two effects are shown to be responsible for this: 1) the radial drift due to the variation of an effective parallel force within orbit width and 2) the non-uniformly evolved orbit width. Simulation using the XGC1 code validates the heat source effect on the generation of $\boldsymbol{E}\times\boldsymbol{B}$ flow shear. Our finding implies that an appropriate implementation of the heat source effect in GK simulations may strongly facilitate the ITB formation. Experimentally, the heat source effect could possibly resolve a long-standing problem in magnetic fusion research exhibiting ITB formation without regard to the q-profile when sufficiently strong power is applied.

There are, of course, missing points in our results due to the simplifications of the source model and turbulence, whose refinements remain as future works. Firstly, a further study regarding the source term θ_{ext} in velocity space is necessary and analytic calculation or numerical simulation with a more realistic source should be performed. Recently, it has been observed a new type of transport barrier by resonant interactions between fast ions created by heating and turbulence [36]. This indicates that the detailed structure of ϑ_{ext} in velocity space is important and should be determined with turbulence in a self-consistent manner. A self-consistent GK simulation with a heating module such as XGC-RF simulation [37], which has been carried out for the study of toroidal flow generation by RF heating, is under consideration to evaluate the heat source effect in more realistic condition. Secondly, the simulation in this work is performed without taking plasma turbulence and the power threshold for the ITB transition is estimated based on a heuristic model. A rigorous demonstration of the ITB formation at a certain threshold power by the heat source effect requires flux-driven turbulence simulations with self-consistently evolving plasma profiles. In fact, this has been a long-standing problem in magnetic fusion community. A full-f GK simulation with turbulence is also under consideration for a further exploration of the heat source effect on ITB formation and confinement scaling.

Finally, we remark that a heat sink can play the same role as the heat source in $\mathbf{E}_r$ generation [19]. In this case, the increament of electric field by the FOW effect can be written as $\Delta E_r = (\tau_c/en_0)\,(\partial S_{sink}/\partial r)$ with a heat sink S_{sink}. As an example, the heat sink near the plasma edge region can be given by $S_{sink} = -\nu_{sink} n_0\,(T_{i0} - T_{i0,edge})$ [38], where ν_{sink} denotes a loss frequency due to some loss mechanism such as radiation and $T_{i0,edge}$ is a temperature at the outer boundary. Considering ν_{sink} with a positive radial gradient in typical L-mode plasmas, a negative $\mathbf{E}_r$ is expected near the edge. In the context of the present work, this implies that the FOW effect in the heat sink region might contribute to the edge transport barrier (ETB) formation. However, since the collisionality is high near the edge, a full-f GK simulation is necessary to investigate

whether the FOW effect contributes to the ETB formation.

Acknowledgments

The authors are grateful to D. H. Park, J. Kim, and J. M. Kwon for helpful discussions. This work was supported by the R&D Program through Korea Institute of Fusion Energy (KFE) funded by the Ministry of Science, ICT and Future Planning of the Republic of Korea (No. KFE-EN2141-7) and by the U. S. Department of Energy under Contract No. DE-AC02-09CH11466. This research used resources of the National Energy Research Scientific Computing Center operated under Contract No. DE-AC02-05CH11231.

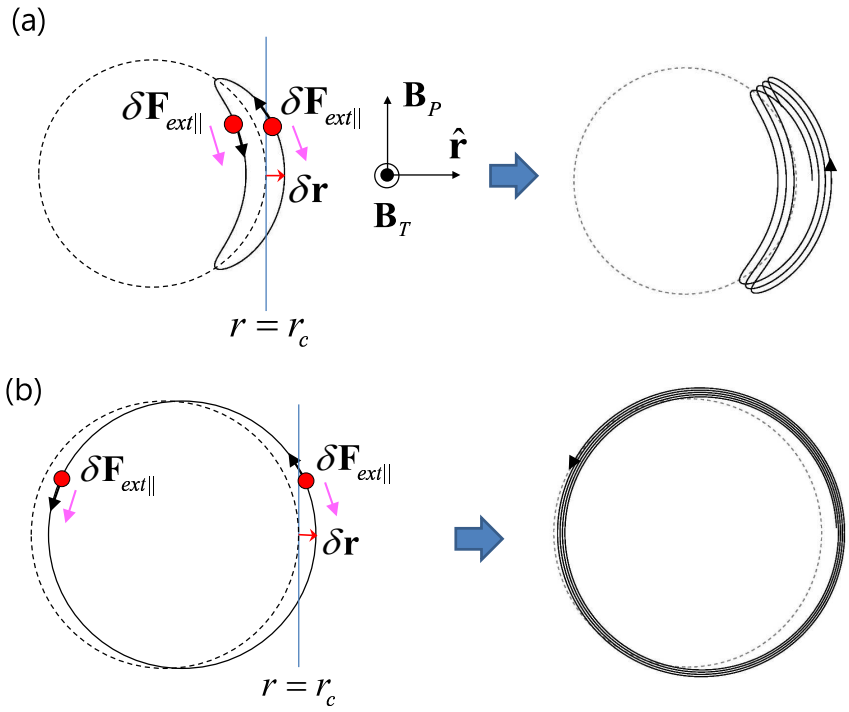

FIG. 1. A schematic diagram for $\delta F_{ext\|}$ in Eq. (10) with $\partial s_h/\partial r < 0$ at $r = r_c$ and outward drifts caused by it for (a) trapped and (b) passing particles.

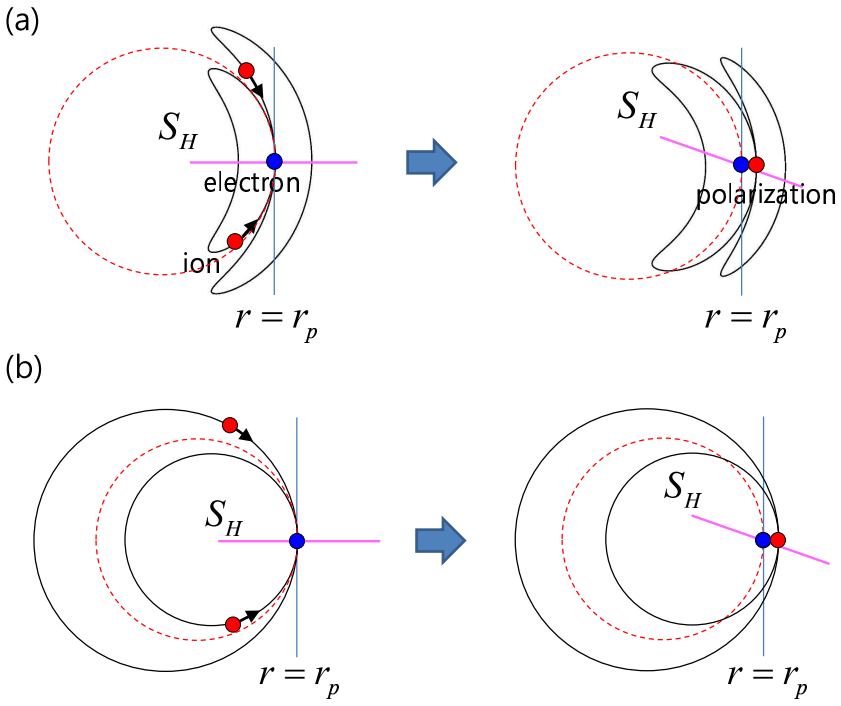

FIG. 2. A schematic diagram showing polarizations induced by δr change due to a non-uniform heat source for (a) trapped and (b) passing particles. Particles inside or outside the $r = r_p$ surface (red dashed line) are more or less heated.

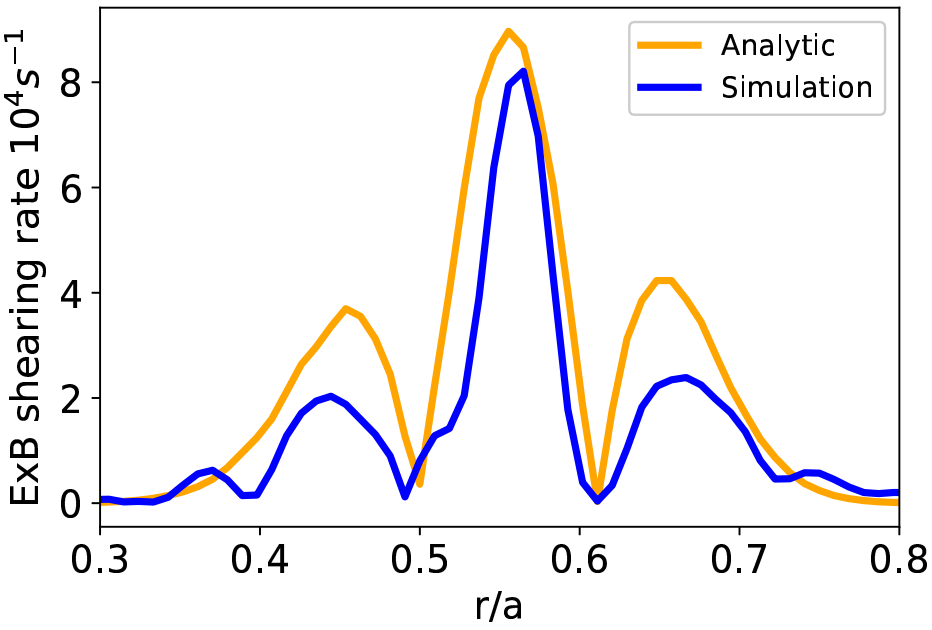

FIG. 3. The generation of $\boldsymbol{E}\times\boldsymbol{B}$ shearing rate (ω_E^H) by external heat sources. Blue and orange lines represent XGC1 simulation and analytic results, respectively.

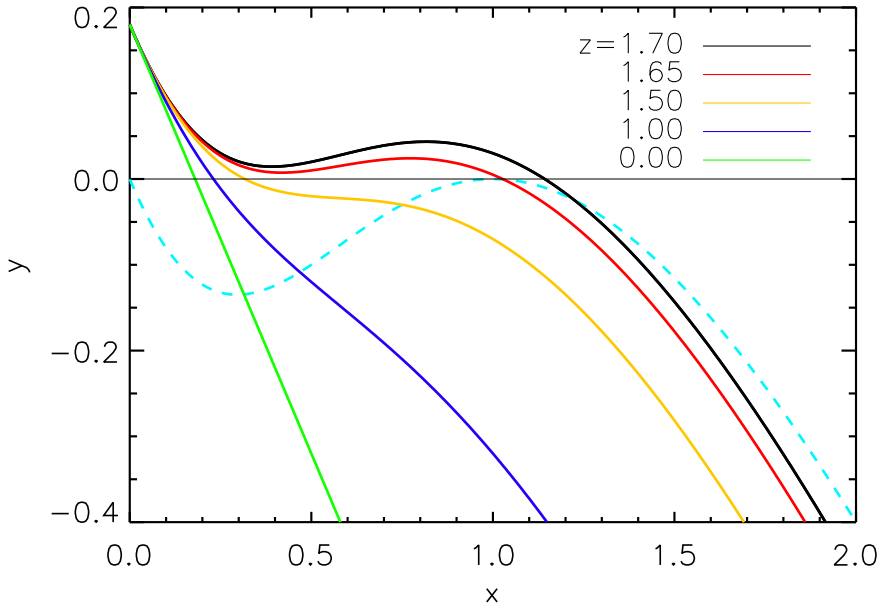

FIG. 4. Dependences of $y = (\tau_c/\gamma_{lin})\,\partial\omega_E/\partial t$ on $x = \omega_E/\gamma_{lin}$ for various $z = \omega^H_{Ec}/\gamma_{lin}$. Solid and dashed lines represent the results with $\eta = 0.18$ and 0, respectively, where $\eta = (\omega_{E0} + \tau_c\Gamma_{NL})/\gamma_{lin}$ with mean flow shearing rate ω_{E0} and nonlinear source Γ_{NL}. For the dashed line, $z = 2$ has been used. In the solid lines, a bifurcation feature, i.e., a sudden increase of ω_E satisfying the steady state condition ($y = 0$) at a critical value of z ($\simeq 1.65$), appears as z or the heating power increases.

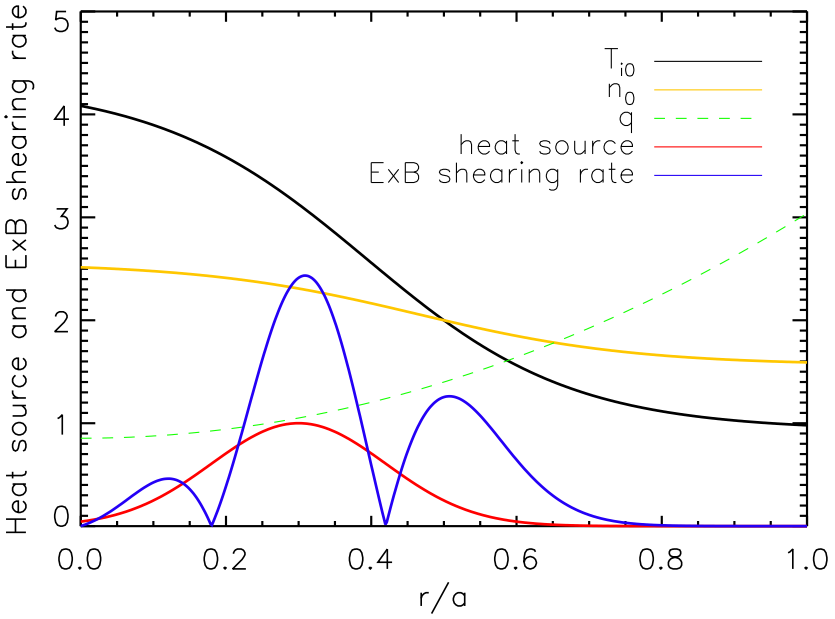

FIG. 5. Profiles of equilibrium ion temperature T_{i0} (keV), density n_0 (10^{19} m^{-3}), safety factor q, and off-axis heat source (S_H/S_0) used in the estimation of threshold power for ITB formation. The blue line represents the $\mathbf{E}\times\mathbf{B}$ shearing rate ω_{Ec}^{H} (10^5 s^{-1}) for an input power $P_{in} = 4.7$ MW.

[1] Wolf R. C. 2003 *Plasma Phys. Control. Fusion* **45**, R1

[2] Wagner F. 2007 *Plasma Phys. Control. Fusion* **49**, B1

[3] Burrell K. H. 2020 *Phys. Plasmas* **27**, 060501

[4] Biglari H., Diamond P. H. and Terry P. W. 1990 *Phys. Fluids B: Plasma Phys.* **2**, 1

[5] Strugarek A., Sarazin Y., Zarzoso D., Abiteboul J., Brun A. S., Cartier-Michaud T., Dif-Pradalier G., Garbet X., Ghendrih Ph., Grandgirard V., Latu G., Passeron C. and Thomine O. 2013 *Phys. Rev. Lett.* **111**, 145001

[6] Chang C. S., Ku S., Tynan G. R., Hager R., Churchill R. M., Cziegler I., Greenwald M., Hubbard A. E. and Hughes J. W. 2017 *Phys. Rev. Lett.* **118**, 175001

[7] Frieman E. A. and Chen L. 1982 *Phys. Fluids* **25**, 502

[8] Brizard A. J. and Hahm T. S. 2007 *Rev. Mod. Phys.* **79**, 421

[9] Ku S., Chang C. S. and Diamond P. H. 2009 *Nucl. Fusion* **49**, 115021

[10] Idomura Y., Urano H., Aiba N. and Tokuda S. 2009 *Nucl. Fusion* **49**, 065029

[11] Görler T., Lapillonne X., Brunner S., Dannert T., Jenko F., Merz F. and Told D. 2011 *J. Comput. Phys.* **230**, 7053

[12] Grandgirard V., Abiteboul J., Bigot J., Cartier-Michaud T., Crouseilles N., Dif-Pradalier G., Ehrlacher Ch., Esteve D., Garbet X., Ghendrih Ph., Latu G., Mehrenberger M., Norscini C., Passeron Ch., Rozar F., Sarazin Y., Sonnendrücker E., Strugarek A. and Zarzoso D. 2016 *Comput. Phys. Commun.* **207**, 35

[13] Obrejan K., Imadera K., Li J.-Q. and Kishimoto Y. 2015 *Plasma Fusion Res.* **10**, 3403042

[14] Levinton F. M., Zarnstorff M. C., Batha S. H., Bell M., Bell R. E., Budny R. V., Bush C., Chang Z., Fredrickson E., Janos A., Manickam J., Ramsey A., Sabbagh S. A., Schmidt G. L., Synakowski E. J. and Taylor G. 1995 *Phys. Rev. Lett.* **75**, 4417

[15] Strait E. J., Lao L. L., Mauel M. E., Rice B. W., Taylor T. S., Burrell K. H., Chu M. S., Lazarus E. A., Osborne T. H., Thompson S. J. and Turnbull A. D. 1995 *Phys. Rev. Lett.* **75**, 4421

[16] Fujita T., Kamada Y., Ishida S., Neyatani Y., Oikawa T., Ide S., Takeji S., Koide Y., Isayama A., Fukuda T., Hatae T., Ishii Y., Ozeki T., Shirai H. and JT-60 Team 1999 *Nucl. Fusion* **39**, 1627

[17] Sakamoto Y., Suzuki T., Ide S., Koide Y., Takenaga H., Kamada Y., Fujita T., Fukuda T., Takizuka T., Shirai H., Oyama N., Miura Y., the JT-60 Team, Hill K. W. and Rewoldt, G. 2004 *Nucl. Fusion* **44**, 876

[18] Sips A. C. C., Baranov Y., Challis C. D., Cottrell G. A., Eriksson L-G., Gormezano C., Gowers C., Greenfield C. M., de Haas J. C. M., von Hellerman M., Huysmans G. T. A., Howman A., König R., Lazarus E. A., Luce T., Nielsen P., O'Brien D., Rice B. W., Sadler G., Söldner F. X., Stamp M. F., Strait E. J., Tubbing B. J. D., Wade M. and Ward, D. J. 1998 *Plasma Phys. Control. Fusion* **40**, 1171

[19] Kim S. S. and Jhang H. 2020 *Phys. Plasmas* **27**, 112302

[20] Parra F. I. and Barnes M. 2015 *Plasma Phys. Control. Fusion* **57**, 045002

[21] Rosenbluth M. N. and Hinton F. L. 1998 *Phys. Rev. Lett.* **80**, 724

[22] Ku S., Chang C. S., Hager R., Churchill R. M., Tynan G. R., Cziegler I., Greenwald M., Hughes J., Parker S. E., Adams M. F., D'Azevedo E. and Worley P. 2018 *Phys. Plasmas* **25**, 056107

[23] Sugama H., Watanabe T.-H. and Horton W. 2007 *Phys. Plasmas* **14**, 022502

[24] Ware A. A. 1970 *Phys. Rev. Lett.* **25**, 15

[25] Sips A. C. C., Peeters A., Ryter F., Wolf R., Greenwald M., Gohil P., Greenfield C., Kinsey J., Barbato E., Bracco G., Buratti P., Esposito B., Baranov Y., Hellsten T., Aniel T., Bécoulet A., Eriksson L., Garbet X., Hoang T., Imbeaux F., Litaudon X., Maget P., Fukuda T., Fujita T., Ide S., Kamada Y., Sakamoto Y., Shirai H., Suzuki T., Takizuka T., Hogeweij D., Esipchuk Y., Ivanov N., Kirneva N., Razumova K., Hahm T., Synakowski E., and Doyle E. 2002 *Plasma Phys. Control. Fusion* **44**, A391

[26] Gohil P., Kinsey J., Parail V., Litaudon X., Fukuda T., Hoang T. *et al* 2003 *Nucl. Fusion* **43**, 708

[27] Connor J. W., Fukuda T., Garbet X., Gormezano C., Mukhovatov V., Wakatani M., the ITB Database Group and the ITPA Topical Group on Transport and Internal Barrier Physics 2004

Nucl. Fusion **44**, R1
[28] Goldston R. J. 1984 *Plasma Phys. Control. Fusion* **26**, 87
[29] Hinton F. L., 1991 *Phys. Fluids B: Plasma Phys.* **3**, 696
[30] Diamond P. H., Itoh S-I, Itoh K., and Hahm T. S. 2005 *Plasma Phys. Control. Fusion* **47**, R35
[31] Waltz R. E., Kerbel G. D. and Milovich J. 1994 *Phys. Plasmas* **1**, 2229
[32] Synakowski E. J., Batha S. H., Beer M. A., Bell M. G., Bell R. E., Budny R. V., Bush C. E., Efthimion P. C., Hahm T. S., Hammett G. W., LeBlanc B., Levinton F., Mazzucato E., Park H., Ramsey A. T., Schmidt G., Rewoldt G., Scott S. D., Taylor G. and Zarnstorff M. C. 1997 *Phys. Plasmas* **4**, 1736
[33] Hinton F. L. and Rosenbluth M. N. 1999 *Plasma Phys. Control. Fusion* **41**, A653
[34] Dimits A. M., Bateman G., Beer M. A., Cohen B. I., Dorland W., Hammett G. W., Kim C., Kinsey J. E., Kotschenreuther M., Kritz A. H., Lao L. L., Mandrekas J., Nevins W. M., Parker S. E., Redd A. J., Shumaker D. E., Sydora R. and Weiland J. 2000 *Phys. Plasmas* **7**, 969
[35] Rewoldt G., Lin Z. and Idomura Y. 2007 *Comput. Phys. Commun.* **177**, 775
[36] Siena A. D., Bilato R., Görler T., Navarro, A. B., Poli E., Bobkov V., Jarema D., Fable E., Angioni C., Kazakov Y. O., Ochoukov R., Schneider P., Weiland M., Jenko F., and the ASDEX Upgrade Team 2021 *Phys. Rev. Lett.* **127**, 025002
[37] Kwon J. M. and Chang C. S. 2008 *International Workshop on e-Science for Physics (Daejeon, Korea, 2008)*
[38] McMillan B. F., Jolliet S., Tran T. M., Villard L., Bottino A., and Angelino P. 2008 *Phys. Plasmas* **15**, 052308